PCCP

PAPER

View Article Online
View Journal | View Issue

Cite this: *Phys. Chem. Chem. Phys.*, 2016, **18**, 11008

Adsorption of PTCDA and C_{60} on KBr(001): electrostatic interaction *versus* electronic hybridization†

Qian Jia,[a] Zhi-Xin Hu,[a] Wei Ji,*[a] Sarah A. Burke,*[b] Hong-Jun Gao,[c] Peter Grütter[d] and Hong Guo[d]

Received 27th December 2015,
Accepted 15th March 2016

DOI: 10.1039/c5cp07999c

www.rsc.org/pccp

The adsorption of functional molecules on insulator surfaces is of great interest to molecular and organic electronics. Here, we present a systematic investigation of the geometric and electronic properties of perylene-3,4,9,10-tetracarboxylic-3,4,9,10-dianhydride (PTCDA) and C_{60} on KBr(001) using density functional theory and non-contact atomic force microscopy to reveal the interplay of interactions between aromatic molecules and insulating substrates. Energetic and structural details are discussed, as well as electronic structures, *e.g.* local electronic density of states, (differential) charge density, and Bader charge analysis, were inspected. Electrostatics was found to be the primary interaction mechanism for systems of PTCDA and C_{60} adsorbed on KBr, which can be further promoted by electronic hybridizations of non-polar, but polarizable, molecules with substrates, *e.g.* C_{60}/KBr(001). Electronic hybridization, depending on the polarizability of the π-system, may be suppressed by introducing high electron affinity atoms, *e.g.* O, into the molecule. Besides, we investigate molecules adsorbed on two-layer KBr(001) covered Cu(001), in which no hybridisation was found between PTCDA and the metal underneath, but a C–Br–Cu hybridized state in C_{60}/KBr(001)/Cu(001). Since the interaction mechanism is dominated by electrostatics, it is concluded that alkali-halides are interesting and important materials for investigation, due to the minor influence on the molecular electronic structure, which may inspire new research fields of electronics.

Introduction

The use of molecules as functional elements in electronic devices is an interesting concept for the continued miniaturization of electronics that has attracted a great deal of attention for several decades.[1–8] While tremendous progress has been made in understanding such systems, it is recognized that molecular electronics is a complicated problem as not only isolated molecules must be understood, but also their assembly, interaction, and contact with the outside world need to be carefully investigated.[2–7] It has been shown in many scanning tunnelling microscopy (STM) studies[3,5,6,9] that interactions with semiconducting and metallic surfaces substantially influence the electronic structure of adsorbed molecules. Since practically viable molecular circuitry is most likely to be self-assembled on solid substrates that are electrically insulating, a critical issue yet to be addressed is how such a molecular layer is influenced by the underlying insulating surface.

Ultrathin insulating films on metal surfaces have been successfully used to image molecules by STM for the past few decades.[10–17] Non-contact atomic force microscopy (NC-AFM) has also been demonstrated as a feasible tool to investigate molecules on bulk insulator surfaces.[18–23] Increasingly, more experimental investigations have thus been focused on easily prepared insulating surfaces or ultrathin films, *e.g.* KBr(001)[24–32] or NaCl(001).[10,11,16,21,31,33–47] However, few efforts have been made to examine the role of insulating crystalline surfaces in the molecular overlayers, especially in terms of the electronic structure. Insulator surfaces are typically considered to have little to no effect on the molecular overlayers, nevertheless, a clear physical picture of how molecule–substrate electronic hybridization is suppressed on insulators has yet to be reported. Furthermore, a comprehensive understanding of the dominant interaction mechanisms for adsorption of molecules on insulating surfaces

[a] *Department of Physics and Beijing Key Laboratory of Optoelectronic Functional Materials & Micro-nano Devices, Renmin University of China, Beijing 100872, China. E-mail: wji@ruc.edu.cn*
[b] *Department of Physics and Astronomy, the Department of Chemistry, and Stewart Blusson Quantum Matter Institute, The University of British Columbia, 6224 Agricultural Road, Vancouver, Canada V6T 1Z1. E-mail: saburke@phas.ubc.ca*
[c] *Institute of Physics, Chinese Academy of Sciences, PO Box 603, Beijing, 100190 China*
[d] *Centre for the Physics of Materials and Department of Physics, McGill University, 3600 rue University, Montreal, Canada H3A 2T8*

† Electronic supplementary information (ESI) available. See DOI: 10.1039/c5cp07999c

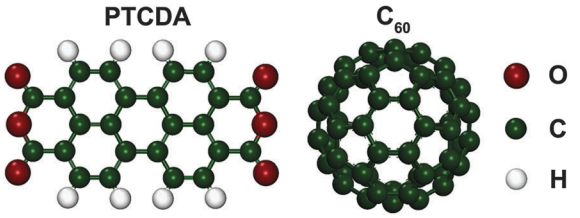

Fig. 1 Ball-stick model showing the atomic structures of PTCDA (left) (right) and C_{60} (left).

is also lacking. Many experiments by means of STM have been conducted on metal substrates covered by a thin insulator layer, *e.g.* alkali halides[43,48,49] or MgO.[50] Such a thin insulator layer helps to decouple the absorbed molecules from the substrate. It would be interesting and important to know if a two-layer-thick insulator is sufficient to electronically isolate the absorbed molecule from the metal substrate.

This work, therefore, endeavours to improve the understanding of the key interactions and influence on the electronic states of adsorbed molecules on ionic surfaces. We have systematically investigated the geometric and electronic structures of C_{60} and perylene-3,4,9,10-tetracarboxylic-3,4,9,10-dianhydride (PTCDA) molecules (see Fig. 1) adsorbed on KBr(001) using density functional theory (DFT) calculations and NC-AFM. The KBr (001) surface is a prototypical insulating surface adopted for investigating molecular overlayers.[24–32] A "polar" molecule, *i.e.* PTCDA, and a nonpolar one, *i.e.* C_{60}, were considered, as they are widely investigated and representative molecules in molecular electronics.[3,5–7,12,26,33,46,51–55] Furthermore, C_{60} and PTCDA adsorbed on KBr(001) have been widely studied experimentally,[24–26,34,35] allowing direct comparison with our modelling results. Note that the term "polar" here does not mean that the centre of the negative charge is separated from that of the positive charge in PTCDA, but refers to the fact that static electrostatic moments (quadrupole in this case), *e.g.* C–O bonds, are polarized. The molecule/2ML KBr(001)/Cu(001) system is adopted to describe issues of whether the hybridization was formed between molecules and metal substrates.

In the following, DFT calculations with the dispersion correction (DFT-D2)[56,57] were used to reveal the most likely adsorption configuration for each system and compared with our NC-AFM experiments, which also took van der Waals interaction into account. The adsorption energy and structural details were discussed. Given the adsorption configuration, electronic structures, *e.g.* local density of states (LDOS), were calculated to analyse the details of electronic hybridization, from which electrostatics was implicated as the primary interaction between the molecules and the substrate. We find that the highest occupied molecular orbitals (HOMOs) of C_{60} electronically hybridize with the Br p-state of the KBr substrate, forming a few new states; this is in contrast to PTCDA/KBr where there is no appreciable molecule–substrate electronic hybridization. Further proof, including differential charge density (DCD), real space distribution of wavefunctions, and structural distortions, supports a predominately electrostatic driven interaction, which does not change even with the inclusion of a Cu substrate under a bilayer of KBr(001). By investigating these two distinctly different molecules on a widely adopted substrate KBr, our results shed considerable light on improving the knowledge of the interplay of functional molecules and insulator surfaces. Furthermore, we inferred several general features for the influences of insulator surfaces on molecular overlayers by comparing C_{60}/KBr with PTCDA/KBr, which is expected to assist in choosing appropriate molecules and substrates for molecular nanoelectronics.

Computational details

Density functional theory calculations were carried out using the standard DFT-Projector-Augmented-Wave (DFT-PAW) method[58] with the Perdew–Burke–Ernzerhof (PBE) functional[59] and the revised form of the RPBE functional[60] for exchange–correlation energy and a planewave basis set with the kinetic energy cutoff up to 400 eV, as implemented in the Vienna *Ab nitio* Simulation Package (VASP).[61,62] Semi-core p electrons of K were treated as valence electrons. Five alkali halide layers, separated by a vacuum slab equivalent to seven alkali-halide layer thickness (23 Å), were employed to model the surface. The two bottom layers were kept fixed during structural relaxations and all other atoms were fully relaxed until the net force on every relaxed atom is less than 0.01 eV $Å^{-1}$. A 2×3 and a 3×3 supercell were employed to model the PTCDA/KBr monolayer and a 4×4 one to approximately simulate the 8×3 C_{60}/KBr monolayer which is one of the structures observed for C_{60} on KBr.[25] The surface Brillouin zone of both categories of supercells was sampled by a $2 \times 2 \times 1$ for the relaxation and a $4 \times 4 \times 1$ k-point grid for the total energy calculation to ensure the convergence of total energy better than 1 meV per atom. A dispersion correction in the form of DFT-G06[56] was applied to PBE (PBE-D) and RPBE (RPBE-D) functionals, respectively. Both methods use the same global scaling factor s_6, the damping parameter d and the cutoff radius for pair interactions as those for the PBE functional in our calculations. It was demonstrated that RPBE-D is one of the most suitable methods for modeling molecule–metal interfaces among various GGA, DFT-D and vdW-DF functionals.[63] We expected that RPBE-D also performs well for modeling molecule–insulator interfaces, since the molecule–surface interacting potentials on metal and insulator surfaces are both in a r^{-3} form.[64] We have checked the adsorption of a series of small molecules including CH_3, H_2O, and CO_2 on an alkali halide substrate (unpublished data). It is demonstrated that the RPBE-D method performs well for small molecules adsorbed on insulating surfaces. In the rest of this paper, we thus focused on the results of RPBE-D while those of PBE were also reported for comparison.

Results and discussion

Atomic structures

PTCDA/KBr(001). A recent literature study indicates that the cation-carboxylic-O interaction primarily contributes to the molecule–substrate interaction for PTCDA adsorbed on

alkali-halide surfaces.[33,35,37,43] We thus considered adsorption sites where the carboxylic-oxygens (denoted as O1) are near K cations. In terms of a single PTCDA adsorbed on KBr, the three most energetically favoured adsorption configurations were selected among the combinations of four adsorption sites and two adsorption orientations. They are Br-Top, Hollow, and Br-Top-R45, as shown in Fig. 2(a). Configuration Br-Top is the most stable one among the three, as shown in Table 1. Moreover, vertically stable configurations were considered for single PTCDA on KBr. It is demonstrated that the Br-Top is still the most stable configuration and non-covalent bonding was formed between Br and O atoms. Detailed structural discussion is available in Part 1 in the ESI.†

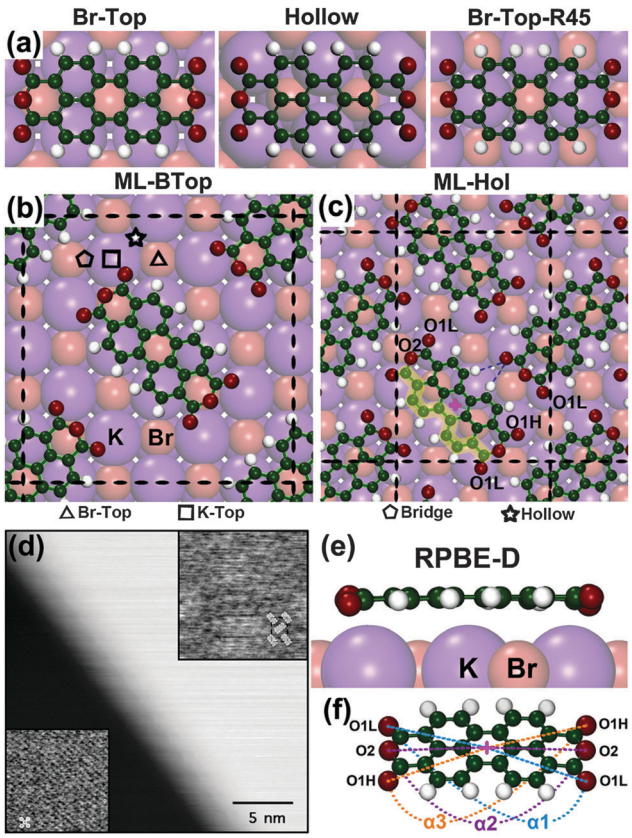

Fig. 2 Top views of RPBE-D functional optimized structures in single-molecular configurations (a) and in monolayered configurations (b) and (c), in which these two supercells are marked by the black dashed lines. The K and Br atoms are represented by larger purple and smaller brown spheres, respectively. The "triangle", "square", "pentagon", and "star" represent the adsorption sites right on top of Br (Br-Top) and K (K-Top) atoms, in between of K and its adjacent Br and at the center of the square made by two Br and two K atoms in (b). The center of a PTCDA is indicated by a pink "+" in (c) and O1L, O1H, and O2 refer to lower and higher-carboxylic O and anhydride O, respectively. The yellow shadow refers to the over-K C atom, denoted as C_{edge}. Other C atoms, which are over Br atoms, are denoted as C_{mid}. Two blue thin dashed lines in (c) show likely hydrogen bonds between two PTCDAs. (d) NC-AFM image of the multilayered PTCDA island on KBr (25 nm × 25 nm, Δf = 22.5 Hz, and full z-scale 1.33 nm), inset contrasts are adjusted to show KBr lattice resolution lower left and PTCDA lattice upper right, with overlay of unit cells on each. Side views of the RPBE-D fully relaxed monolayer structure (ML-Hol) are shown in (e). (f) gives the angles mentioned in Table 2.

The most favourable adsorption site changes when PTCDA molecules form a monolayer. Two monolayer configurations were considered for comparison, *i.e.*, Br-Top (the most favoured adsorption site among all the single-molecule configurations) and Hollow (the most compact one among all the monolayer configurations), denoted as ML-BTop and ML-Hol, respectively (Fig. 2(b) and (c)). The smallest supercell for ML-BTop is a 3 × 3 one, while configuration ML-Hol only requires a smaller 2 × 3 supercell. Configuration ML-Hol is, therefore, the theoretically suggested monolayer configuration according to Table 1.

Fig. 2(c) shows the geometry of configuration ML-Hol, in which the central phenyl ring of a PTCDA, marked as a pink cross, resides at the hollow site of two Br anions and two K cations. Four O atoms located on the top of four K cations are denoted as O1. The rest two O atoms are denoted as O2. All C atoms of a PTCDA can be classified into two categories, *i.e.* two arm-chair edges, one of which is marked with a yellow shadow bar and two C–C bonds. Each arm-chair edge contains 10 carbon atoms, located on top of K cations (over-K C atoms). The two C–C bonds are comprised of four carbon atoms, in the middle of a PTCDA where C atoms are over Br anions (over-Br C atoms).

Fig. 2(d) shows a NC-AFM image of PTCDA/KBr, acquired at the edge of a PTCDA island. It shows the atomically resolved KBr surface and the molecularly resolved PTCDA island. The PTCDA lattice measured relative to KBr suggests a p(2 × 3) superstructure with PTCDA molecules oriented along {110} directions of the KBr lattice. The shape of the supercell and molecular orientation within the overlayer observed by NC-AFM are highly consistent with the theoretically predicted configuration ML-Hol. The theoretically revealed adsorption sites and geometries, together with experimental observations, compellingly indicate ML-Hol configuration as the most favourable structure of PTCDA islands on KBr(001).

Fig. 2(e) shows the side view of a fully relaxed PTCDA in configuration ML-Hol. The relaxed structure using either RPBE-D or PBE indicates a bent PTCDA that the vertical positions of the four O1 atoms are slightly lower than those of the almost planar perylene core, similar to PTCDA/Ag(111).[54] As PTCDA is a symmetric molecule, the four O1 atoms shall be identical. However, when these molecules aggregate into a monolayer, a symmetry breaking was found that the four O1 atoms diagonally split into two categories. Table 2 shows the details of calculated angles and molecule–substrate distances of monolayer PTCDA/KBr. One is 0.25 Å (0.30 Å, PBE value, the same hereinafter) vertically higher than the other. We denote the higher one as O1H and the lower one as O1L, as shown in Fig. 2(c). Three angles, namely α_1, α_2, and α_3 shown in Fig. 2(f) and Table 2, are available to reflect the bending of PTCDA. The value of angle α_3, nearly 180°, is significantly larger than that of angle α_1, a result of the higher vertical position of O1H than that of O1L, most likely ascribed to the two hydrogen bonds (O–H distance of 2.82 Å and 2.92 Å) formed between an O1H and two H atoms of an adjacent PTCDA, marked by the thinner navy dashed lines in Fig. 2(c).

C_{60}/KBr(001). We considered 18 configurations of C_{60}/KBr based on four adsorption sites of the KBr surface, three contact positions of C_{60}, *i.e.* pentagon, hexagon, and double-bond, and

Table 1 The PBE, RPBE-D and PBE-D results of the adsorption energies and their differences of a single PTCDA on KBr(001), the PTCDA monolayer and the C_{60} monolayer on KBr(001). In terms of PTCDA/KBr(001), the results of configuration 3 × 3 ML-BTop were renormalized to a 2 × 3 supercell in order to be energetically comparable with those of ML-Hol

	PTCDA/KBr(001)								
	Single PTCDA			PTCDA monolayer (per molecule)			C_{60}/KBr(001)		
Adsorption energy	Br-Top	Hollow	Br-Top-R45	ML-BTop	ML-Hol	ML-Hol–ML-BTop	$C_{60\text{-DB}}$	$C_{60\text{-Hex}}$	$C_{60\text{-Hex}}$-$C_{60\text{-DB}}$
PBE (eV)	−0.60	−0.20	−0.26	−0.44	−0.58	0.14	−0.04	−0.02	0.02
RPBE-D (eV)	−1.30	−0.80	−0.86	−0.93	−1.27	0.34	−0.39	−0.40	−0.01
PBE-D (eV)	—	—	—	—	—	—	−0.56	−0.63	−0.07

Table 2 Structural details of configuration ML-Hol calculated using PBE and RPBE-D, respectively. α_1, α_2 and α_3 represent the angles O1L–Ctr–O1L, O2–Ctr–O2, and O1H–Ctr–O1H, respectively, in which "Ctr" refers to the center of a PTCDA marked as "+" in Fig. 2(f). Distances d_{O1L-K}, d_{O1H-K}, and $d_{Ctr-surf}$ indicate the distances between O1L and K underneath, O1H and K underneath, and from the center of a PTCDA to the substrate surface, respectively

ML-Hol	α_1 (°)	α_2 (°)	α_3 (°)	d_{O1L-K} (Å)	d_{O1H-K} (Å)	$d_{Ctr-surf}$ (Å)
PBE	174.3	179.8	179.4	3.54	3.87	3.85
RPBE-D	174.8	180.2	178.3	3.36	3.56	3.65

two molecular orientations. As shown in Fig. 3(a) left and right, respectively, two configurations, denoted as C_{60}-Hex and C_{60}-DB, are at least 0.1 eV more stable than the rest, revealed by both PBE and RPBE-D. In contrast to the case of PTCDA/KBr, PBE and RPBE-D suggest two distinct most stable configurations of C_{60}/KBr. In the PBE favoured configuration C_{60}-DB, a double bond, equivalently a roughly 10° rotated pentagon, faces the K cation underneath; while in C_{60}-Hex, the RPBE-D preferred

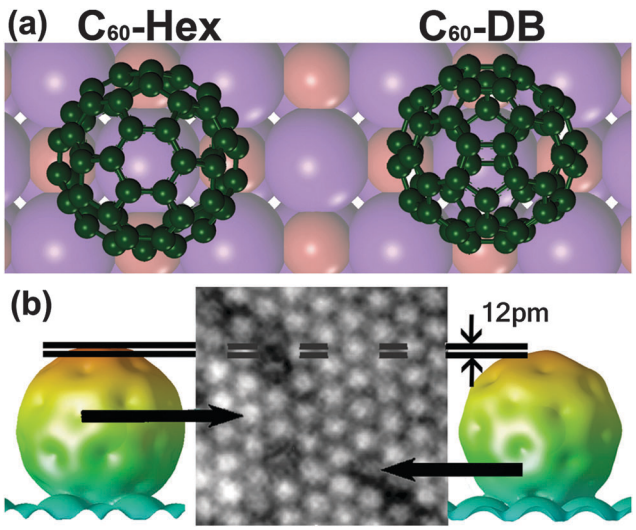

Fig. 3 (a) Top views of the (R)PBE-D and PBE suggest most stable configurations, *i.e.* C_{60}-Hex (left) and C_{60}-DB (right). (b) Isosurfaces (0.01 e Å^{-3}) of the calculated total charge densities of C_{60}-Hex (left) and C_{60}-DB (right), in comparison with a NC-AFM image. The colors of the isosurface are mapped to the height in the *z* direction (from surface towards vacuum). The middle panel shows a NC-AFM image of the monolayered C_{60} island on KBr(001). "Bright" and "dim" spots (see middle) represent C_{60}-Hex and C_{60}-DB, respectively.

configuration, a hexagon of the C_{60} is in contact with the K cation underneath. Another functional, *i.e.* PBE-G06 (PBE-D), is adopted to clarify the issue of which method is more reliable. Although PBE shows that C_{60}-DB is 0.02 eV more stable than C_{60}-Hex, either of the other two dispersion-corrected functionals indicates a slightly more stable C_{60}-Hex according to Table 1. Structural details of the two most stable configurations for C_{60}/KBr are summarized in Table S1 and Part 2 in the ESI,† which shows the negligible structural difference calculated by PBE, PBE-D and RPBE-D.

These two nearly energetically degenerated molecular configurations are consistent with early AFM experiments where two types of molecules were observed.[24,25] The apparent height of C_{60}-Hex in simulated NC-AFM images is at least 12 pm higher than that of C_{60}-DB according to the charge density contour. Both the fact that more "bright" and comparatively few "dim" molecules, as well as the height difference of 21 pm[24,25] are consistent with the theoretical findings in this report.

Electronic structures. Local partial density of states (LPDOS) of PTCDA/KBr (in configuration ML-Hol) and C_{60}/KBr (in configuration C_{60}-Hex), calculated with RPBE-D, are shown in Fig. 4(a) and (b), which are qualitatively the same as those with the PBE functional. More extensive discussions on the effect of vdW correction to LPDOS were conducted in Part 2 of the ESI,† which shows that the features obtained by empirical and self-consistent vdW methods coincide with each other. Visualized wavefunctions of the highest occupied molecular orbitals (HOMOs) and the lowest unoccupied molecular orbitals (LUMOs) of PTCDA and C_{60} after adsorption are also discussed in this subsection.

Non-hybridized PTCDA on KBr. LPDOS of O1 (carboxylic O), C, and Br atoms of PTCDA/KBr before and after adsorption are shown in Fig. 4(a). It was found that the gap between HOMO−1 and the HOMO of an adsorbed PTCDA is 0.3 eV larger than that of a bare PTCDA, but other gaps between two adjacent higher-energy MOs, in particular the HOMO–LUMO gap, do not change. These results suggest that the electronic structure of PTCDA does not appear to be significantly influenced by the KBr substrate. Specifically, the molecular states of PTCDA do not hybridize to substrate states in any appreciable way. The HOMO of the adsorbed PTCDA is situated at roughly 0.3 eV lower than the upper-edge of the Br p band (∼−6.7 eV), not aligning to the band edge. This band edge does not appreciably move (only several meV), before and after the adsorption. All these results suggest that the charge transfer between PTCDA

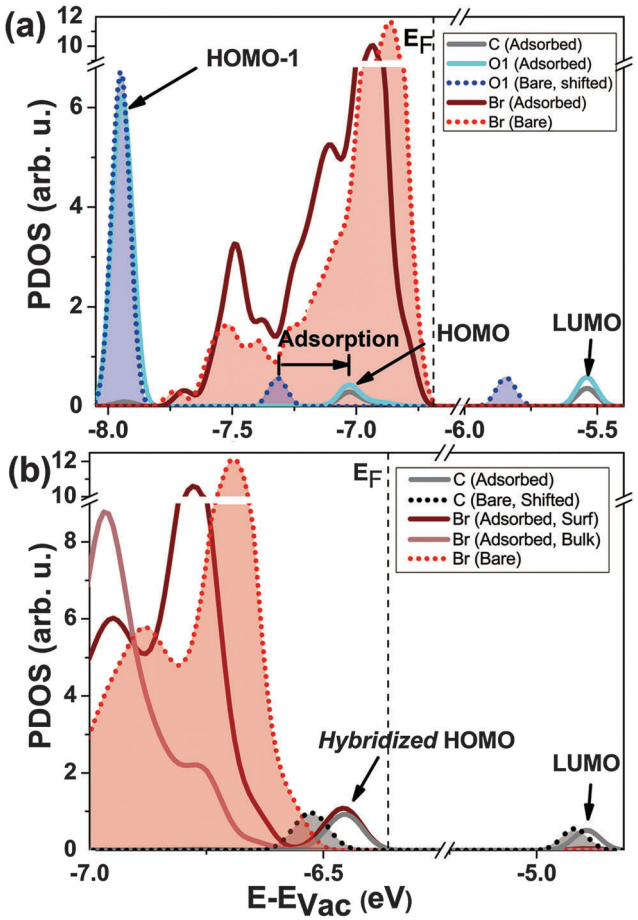

Fig. 4 (a) Local partial density of states for a carboxylic oxygen (O1) and an "averaged" C atom in PTCDA, and a Br anion under C atoms in PTCDA/KBr, shown in (a) and for a C atom in the bottom hexagon layer of C_{60} and a Br underneath in C_{60}/KBr, shown in (b). All energies are referenced to the vacuum level (hereinafter). All states of the bare molecule and the bare substrate are plotted using dotted lines with shadows, while the states after adsorption are all in solid lines. Some molecular orbitals are indicated by the black arrows. "E_F" here refers to the energy of the highest occupied state.

and KBr is very small, in other words, no covalent bond was formed between the molecule and the substrate, which was confirmed by the differential charge density and Bader charge analysis discussed in the "Interaction mechanism" section.

Hybridization between C_{60} and KBr. We plotted the PLDOS of a C atom in the bottom layer of C_{60} and one of the four Br anions underneath for C_{60}/KBr(001) in Fig. 4(b). It unambiguously shows a C–Br hybridized state, in contrast to the PTCDA/KBr case where no molecule–substrate electronic hybridization was found. The hybridized HOMO state, sitting at −6.45 eV, is comprised of the molecular HOMO and a surface Br state, whereas bulk states of Br (light brown solid line) do not contribute to it. The adsorption of C_{60} lowers the work function of bare KBr(001) by 0.1 eV, resulting in an upward shift of the upper edge of the occupied states.

The HOMO–LUMO gap of the adsorbed C_{60} (gray solid line) is 0.04 eV smaller than that of a bare one (black dotted line), which is due to the adsorption-induced upward shift of C_{60}'s HOMO. These results, combined with the slightly downward shifted edge of the surface Br p band, suggest a charge transfer of 0.04 *e* (see the Bader charge analysis section) from KBr to C_{60}, consistent with the electron-acceptor nature of C_{60}.[65–68]

Real space distribution of electronic states. Electronic states near band gaps are of particular interest for molecular electronics. We thus plotted visualised wavefunctions of a few states originating from HOMOs and LUMOs of C_{60} and PTCDA, to illustrate the electronic hybridization found between C_{60} and KBr and the electronically inert PTCDA/KBr interface. Fig. 5(a) and (b) show the hybridized HOMO of C_{60} residing at −6.45 eV and the LUMO locating at −4.86 eV, respectively, which are consistent with the LPDOSs in Fig. 4. Interestingly, the LUMO of C_{60} does not hybridize with the substrate, and hence it retains its original shape and energy. On the other hand, as shown in Fig. 5(c) and (d), neither PTCDA's HOMO nor its LUMO electronically interacts with KBr since there is no electron distribution on the substrate for these specific molecular states. Those facts are, again, consistent with the hybridization section when we analysed LPDOSs.

Strength of hybridization. An interesting question thus arises: why does C_{60} hybridize with KBr but PTCDA does not? A key difference between these two molecules is that oxygen has a higher electron affinity than carbon, which significantly reduces the polarizability of the π-electron system (perylene core) of PTCDA by drawing electrons towards these O atoms. The reduced polarizability suppresses the ability of electronic hybridization, resulting in less reactive C atoms for the frontier MOs.[52] Although oxygen atoms in PTCDA have the possibility to hybridize with substrate Br to form covalent-like Br–O bonds, electronic hybridization between Br and O is unlikely, due to the high electron affinity of both Br and O. These negatively charged atoms effectively lead to a repulsive electrostatic interaction rather than an attractive one. Unlike PTCDA, C_{60} has a rather uniform electron distribution resulting in the π-electrons having a significant polarizability, which promotes the hybridization between the C atoms and substrate Br. These findings suggest that the polarizability of molecules largely determines the strength of electronic hybridization between molecules and alkali-halides.

Non-hybridization of PTCDA/2ML KBr(001)/Cu(001). We calculated the electronic structure of a PTCDA monolayer adsorbed on a 2ML-KBr-covered Cu(001) surface. The lattice mismatch between KBr and Cu(001) is 6.8%. The C_{60} case was not considered because of the fact that C atoms already hybridized with KBr layers without introducing any metal substrate.

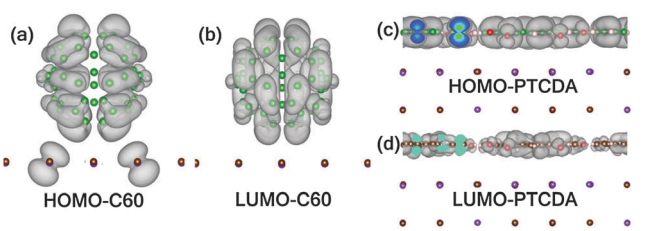

Fig. 5 Real space distributions of wavefunctions of HOMO (a) and LUMO (b) of C_{60}/KBr; and HOMO (c) and LUMO (d) of PTCDA/KBr.

Our results suggest that there are no new hybridized states between PTCDA and 2ML-KBr or Cu atoms. This indicates that two-layer alkali halides are good candidate materials for decoupling previously observed PTCDA-metal covalent bonding.[54] A detailed discussion of the electronic structures of PTCDA and C_{60} adsorbed on two layer KBr(001) sitting on the Cu metal substrate can be found in Part 3 in the ESI.† We also simulated the STM images of PTCDA- and C_{60}-covered 2ML-KBr thin films on copper surfaces, which not only is highly consistent with the electronic structure discussion, but also agrees with similar STM experiments. More discussions are available in Part 4 in the ESI.†

Interaction mechanism. The interaction mechanism between functional molecules and substrates is of great importance to adsorption behaviours. In this subsection, two kinds of electrostatic interaction mechanisms, distinguished by whether it was electronic hybridization enhanced, were revealed for PTCDA/KBr and C_{60}/KBr, respectively, according to differential charge density, Bader change analysis, and structural distortions upon adsorption. All the calculations in this subsection were performed using the RPBE-D method if not specified.

Differential charge density. Differential charge density (DCD) is defined as $\rho_{DCD} = \rho_{Total} - \rho_{Molecule} - \rho_{Substrate}$. Fig. 6(a) and (b) show the DCDs of PTCDA/KBr at the two slabs illustrated in the associated lower panels, respectively. Charge accumulation (warm colours) around O1 and C_{edge} and charge reduction (cold colours) of the O2 and C_{mid} are explicitly shown in Fig. 6(a) where the charge density slab is slightly below PTCDA molecules. Opposite features were found in the DCD of a slab close to the substrate (Fig. 6(b)), *i.e.*, slight charge reduction of the surface K cations below O1 atoms and significant charge accumulation around the Br anions under O2 and C_{mid} atoms. In a slab near C_{60} (Fig. 6(c)), strong charge accumulation was found around the lowest hexagon of C_{60}, while slight charge reduction was observable below the higher C atoms. In terms of the slab right above the substrate (Fig. 6(d)), tiny charge accumulation is appreciable over a K cation (at the center of the panel) and relatively large charge accumulation appears around the Br anions adjacent to the said K cation.

All the DCDs share the same feature that charge accumulation and reduction are vertically superposed for both PTCDA and C_{60} adsorbed on KBr, which unambiguously suggests an electrostatic mechanism for the molecule–substrate interaction. In terms of PTCDA/KBr, such a mechanism concluded the primary interaction for the interface, since there was no appreciable electronic hybridization between PTCDA and KBr. Although electronic hybridization was found in C_{60}/KBr, it induces the charge redistribution, largely enhancing the strength of electrostatic interactions. The electrostatic interaction is, therefore, a very important portion for the interface interaction. The resulted Bader charge analysis and surface structural distortion support these statements.

Bader charge analysis. Bader charge analysis[69] was employed to quantitatively investigate DCD-suggested charge redistribution and likely molecule–substrate charge transfer. In general, Fig. 7(a) illustrates the charge redistribution of PTCDA/KBr, in which electrons relocate from the H atoms (green balls) to C_{edge} atoms (red balls). Such electron redistribution is ascribed to the presence of the K cations underneath offering extra electron-attractive potential, which strengthens the electrostatic interaction. The C_{mid} and O2 atoms are essentially neutral, *i.e.*, the gained or lost electrons are almost balanced. All "green balls" lose a total charge of 0.22 *e* per molecule (all referring to "per molecule" hereinafter). Meanwhile, 0.30 *e* is gained by all "red balls". An extra 0.08 *e* was donated by the substrate, primarily surface Br anions.

Internal charge redistribution occurs throughout C_{60} with an amount of 0.04 *e* transferred from the substrate. In particular, the four Br anions, marked with black stars in Fig. 7(b), are consistent with the conclusion that electrons transferred from Br

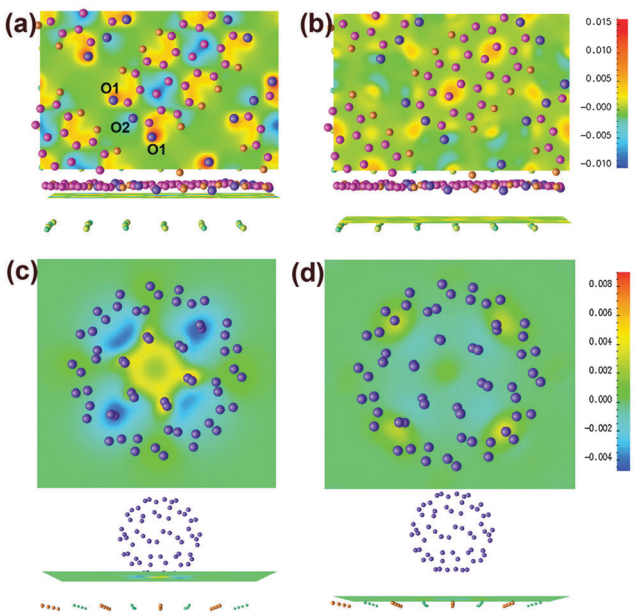

Fig. 6 Top views (upper) and side views (lower) of DCDs of PTCDA/KBr(001) in slabs near molecules (a) and the substrate (b); and those of C_{60}/KBr(001) in slabs just below the molecule (c) and just above the substrate (d). The colors are mapped by the DCD values, in units of e $Å^{-3}$, as illustrated by the color bars.

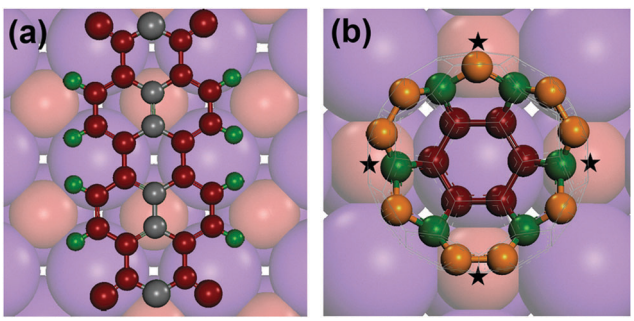

Fig. 7 Sketches of charge variations of PTCDA (a) and C_{60} (b) on KBr between before and after the adsorption. Green, gray, and red (orange) balls represent the electron losses, neutral, and electron gains during adsorption. Only several bottom carbon atoms of C_{60} are shown in ball-stick style in (b), where four Br anions are marked with black stars.

to C atoms made in the C–Br electronic hybridization section. In a C_{60} molecule, the first (red balls in Fig. 7(b)) and third layer (orange balls) gain 0.05 *e* and 0.04 *e*, respectively, while the second layer (green balls), in between those two electron-gained layers, loses 0.04 *e*. The alternating appearance of gaining and losing electron was also found in the fourth to sixth layer, lowering the total energy of C_{60} due to electrostatic attraction. Moreover, additionally gained negative charge in the bottom layer of C_{60} attracts the K cation underneath, further strengthening the molecule–substrate interaction. All these facts manifest that electrostatic interaction, promoted by electronic hybridizations, takes primary responsibility for the C_{60}/KBr system, in accordance with the DCD results. The Bader analyses for molecules adsorbed on the 2ML-KBr-covered Cu substrate are discussed in Part 5 in the ESI.†

Structural distortion of the substrate. Fig. 8 illustrates the molecule-adsorption-induced structural distortions of the KBr substrate. A half of absorbed PTCDA and the associated substrate atoms underneath are shown in Fig. 8(a) and (b). The two O1 atoms effectively attract the two K cations underneath, leading to the K cations being pulled up from their initial positions by 0.06 Å along the directions indicated by the black arrows in Fig. 8(a). Vertical distortions were also found for K cations, with 0.10 Å (0.09 Å for PBE) upwards, and 0.05 Å (0.02 Å for PBE) downwards for Br anions, as shown in Fig. 8(b). Both vertical shifts are significant compared with any anticipated rumpling of the KBr(001).[70] The upward shift of K cations is a result of the strong attraction between the K cations and negatively charged O1 atoms, and the repulsion between the first-layer Br anions and C atoms pushes the Br anions into the surface.

Similar to the PTCDA's case, the repulsion between the Br anions and C atoms pushes these Br anions under the C_{60} outwards, as indicated by black arrows in Fig. 8(c). Fig. 8(d) shows that these four Br anions are also vertically lowered by 0.08 Å (0.06 Å for PBE), which is, again, ascribed to the Br–C repulsion. The more positive K cation below C_{60} moves downwards by 0.06 Å (0.09 Å for PBE), owing to a strengthened electrostatic attraction between the K cation and adjacent Br anions. All these distortions were induced to favour molecule–substrate electrostatic interaction, which implies, again, that electrostatics should be responsible for the primary interaction of these interfaces.

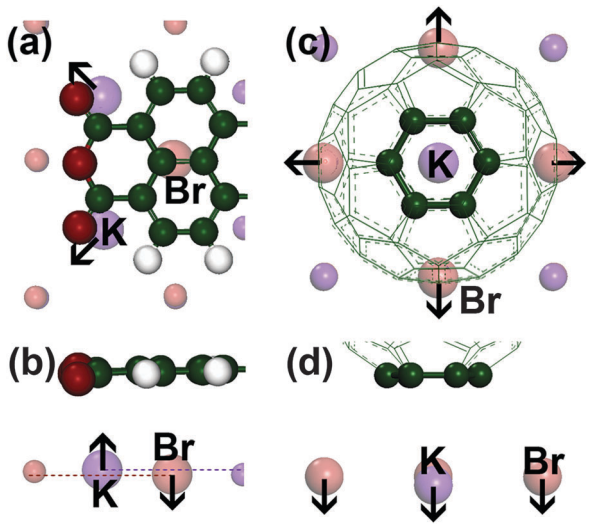

Fig. 8 Structural distortions of K cations and Br anions at the interface during the adsorption of PTCDA (a) and (b) and C_{60} (c) and (d) in top views (a) and (c) and side views (b) and (d). All larger balls in substrates, together with black arrows, are considered in discussion. The direction of these black arrows indicates the direction of movement for the associated atoms.

Conclusions

In summary, we determined the most likely configurations for single molecule and monolayer PTCDA/KBr(001), and a flat-lying hexagonal and a tilted pentagonal configuration for C_{60}/KBr(001). We indicate that the primary interaction mechanism for both PTCDA and C_{60} adsorbed on KBr is electrostatics, which can be further strengthened by electronic hybridizations between non-polar molecules, *e.g.* C_{60}, and alkali-halide substrates. The hybridization, depending on the polarizability of the π-system, can be suppressed by introducing high electron affinity atoms, *e.g.* O, into the π-system. The found internal charge redistribution at the molecule–substrate interfaces for both systems is a response to the periodic electrostatic potential generated by Br anions and K cations on the KBr surface. When we consider the adsorption on the insulating layer-covered metal substrate, no oxygen-metal hybridized state was found for PTCDA/2ML-KBr(001)/Cu(001), but a C–Br–Cu hybridized state was detected for C_{60}/2ML-KBr(001)/Cu(001).

Due to the dominant electrostatic interaction mechanism, we conclude that alkali-halides are competitive candidate materials which could be adopted to support low polarizability molecules, *e.g.* PTCDA, in future electronics. In terms of high polarizability molecules, like C_{60}, side groups or other introduced high electron affinity atoms were expected to help preventing or even tuning the hybridization. It would be thus interesting to explore the role of alkali halides in other purely carbon based π-systems, like graphene and its nanoribbons, and the role of substrate-induced internal charge redistribution in electron transport properties in future studies.

Acknowledgements

We gratefully acknowledge financial support from the National Natural Science Foundation of China (NSFC), under Grant No. 11004244, 11274380 and 91433103, and The Ministry of Science and Technology (MOST) of China under Grant No. 2012CB932704 (W. J.). S. B., H. G. and P. G. acknowledge funding from NSERC, FQRNT and CFI. We are grateful to the Physics Lab for High-Performance Computing of RUC, Shanghai Supercomputing Center and CLUMEQ for substantial computer time.

Notes and references

1 A. Aviram and M. A. Ratner, *Chem. Phys. Lett.*, 1974, **29**, 277–283.
2 C. Joachim, J. K. Gimzewski and A. Aviram, *Nature*, 2000, **408**, 541–548.

3 S. M. Barlow and R. Raval, *Surf. Sci. Rep.*, 2003, **50**, 201–341.
4 M. A. Reed and T. Lee, *Molecular nanoelectronics*, Amer Scientific Pub., 2003.
5 F. Rosei, M. Schunack, Y. Naitoh, P. Jiang, A. Gourdon, E. Laegsgaard, I. Stensgaard, C. Joachim and F. Besenbacher, *Prog. Surf. Sci.*, 2003, **71**, 95–146.
6 N. Papageorgiou, E. Salomon, T. Angot, J.-M. Layet, L. Giovanelli and G. L. Lay, *Prog. Surf. Sci.*, 2004, **77**, 139–170.
7 J. Fraxedas, *Molecular organic materials: from molecules to crystalline solids*, Cambridge University Press, 2006.
8 F. Mohn, J. Repp, L. Gross, G. Meyer, M. S. Dyer and M. Persson, *Phys. Rev. Lett.*, 2010, **105**, 266102.
9 T. Brumme, O. A. Neucheva, C. Toher, R. Gutiérrez, C. Weiss, R. Temirov, A. Greuling, M. Kaczmarski, M. Rohlfing and F. S. Tautz, *Phys. Rev. B: Condens. Matter Mater. Phys.*, 2011, **84**, 115449.
10 G. V. Nazin, X. H. Qiu and W. Ho, *Phys. Rev. Lett.*, 2005, **95**, 166103.
11 J. Repp, G. Meyer, S. M. Stojković, A. Gourdon and C. Joachim, *Phys. Rev. Lett.*, 2005, **94**, 026803.
12 B. Such, G. Goryl, S. Godlewski, J. J. Kolodziej and M. Szymonski, *Nanotechnology*, 2008, **19**, 475705.
13 M. Mura, A. Gulans, T. Thonhauser and L. Kantorovich, *Phys. Chem. Chem. Phys.*, 2010, **12**, 4759–4767.
14 Z. Li, H. Y. Chen, K. Schouteden, K. Lauwaet, L. Giordano, M. I. Trioni, E. Janssens, V. Iancu, C. Van Haesendonck and P. Lievens, *Phys. Rev. Lett.*, 2014, **112**, 026102.
15 G. Meyer, L. Gross, F. Mohn and J. Repp, *Chimia*, 2012, **66**, 10–15.
16 I. Swart, T. Sonnleitner, J. Niedenführ and J. Repp, *Nano Lett.*, 2012, **12**, 1070–1074.
17 L. Gao, Z. Deng, W. Ji, X. Lin, Z. Cheng, X. He, D. Shi and H. J. Gao, *Phys. Rev. B: Condens. Matter Mater. Phys.*, 2006, **73**, 075424.
18 Y. Qi, *Surf. Sci. Rep.*, 2011, **66**, 379–393.
19 J. M. LeDue, M. Lopez-Ayon, S. A. Burke, Y. Miyahara and P. Grütter, *Nanotechnology*, 2009, **20**, 264018.
20 S. Baumann, I. G. Rau, S. Loth, C. P. Lutz and A. J. Heinrich, *ACS Nano*, 2014, **8**, 1739–1744.
21 F. Mohn, L. Gross, N. Moll and G. Meyer, *Nat. Nanotechnol.*, 2012, **7**, 227–231.
22 F. Mohn, B. Schuler, L. Gross and G. Meyer, *Appl. Phys. Lett.*, 2013, **102**, 073109.
23 P. Rahe, M. Kittelmann, J. L. Neff, M. Nimmrich, M. Reichling, P. Maass and A. Kühnle, *Adv. Mater.*, 2013, **25**, 3948–3956.
24 S. A. Burke, J. M. Mativetsky, S. Fostner and P. Grütter, *Phys. Rev. B: Condens. Matter Mater. Phys.*, 2007, **76**, 035419.
25 S. A. Burke, J. M. Mativetsky, R. Hoffmann and P. Grütter, *Phys. Rev. Lett.*, 2005, **94**, 096102.
26 J. M. Mativetsky, S. A. Burke, S. Fostner and P. Grütter, *Nanotechnology*, 2007, **18**, 105303.
27 L. Nony, E. Gnecco, A. Baratoff, A. Alkauskas, R. Bennewitz, O. Pfeiffer, S. Maier, A. Wetzel, E. Meyer and C. Gerber, *Nano Lett.*, 2004, **4**, 2185–2189.
28 O. H. Pakarinen, J. M. Mativetsky, A. Gulans, M. J. Puska, A. S. Foster and P. Grutter, *Phys. Rev. B: Condens. Matter Mater. Phys.*, 2009, **80**, 085401.
29 R. Pawlak, S. Kawai, S. Fremy, T. Glatzel and E. Meyer, *ACS Nano*, 2011, **5**, 6349–6354.
30 D. S. Wastl, A. J. Weymouth and F. J. Giessibl, *Phys. Rev. B: Condens. Matter Mater. Phys.*, 2013, **87**, 245415.
31 M. Fendrich and T. Kunstmann, *Appl. Phys. Lett.*, 2007, **91**, 023101.
32 J. M. Mativetsky, S. Fostner, S. A. Burke and P. Grutter, *Phys. Rev. B: Condens. Matter Mater. Phys.*, 2009, **80**, 045430.
33 S. A. Burke, W. Ji, J. M. Mativetsky, J. M. Topple, S. Fostner, H. J. Gao, H. Guo and P. Grütter, *Phys. Rev. Lett.*, 2008, **100**, 186104.
34 S. A. Burke, J. M. Topple and P. Grütter, *J. Phys.: Condens. Matter*, 2009, **21**, 423101.
35 J. M. Topple, S. A. Burke, W. Ji, S. Fostner, A. Tekiel and P. Grütter, *J. Phys. Chem. C*, 2011, **115**, 217–224.
36 S. A. Burke, J. M. LeDue, J. M. Topple, S. Fostner and P. Grütter, *Adv. Mater.*, 2009, **21**, 2029–2033.
37 S. A. Burke, J. M. LeDue, Y. Miyahara, J. M. Topple, S. Fostner and P. Grütter, *Nanotechnology*, 2009, **20**, 264012.
38 L. Gross, F. Mohn, P. Liljeroth, J. Repp, F. J. Giessibl and G. Meyer, *Science*, 2009, **324**, 1428–1431.
39 L. Gross, F. Mohn, N. Moll, G. Meyer, R. Ebel, W. M. Abdel-Mageed and M. Jaspars, *Nat. Chem.*, 2010, **2**, 821–825.
40 L. Gross, N. Moll, F. Mohn, A. Curioni, G. Meyer, F. Hanke and M. Persson, *Phys. Rev. Lett.*, 2011, **107**, 086101.
41 F. Mohn, L. Gross and G. Meyer, *Appl. Phys. Lett.*, 2011, **99**, 053106.
42 J. M. Topple, S. A. Burke, S. Fostner and P. Grütter, *Phys. Rev. B: Condens. Matter Mater. Phys.*, 2009, **79**, 205414.
43 H. Karacuban, S. Koch, M. Fendrich, T. Wagner and R. Möller, *Nanotechnology*, 2011, **22**, 295305.
44 T. Trevethan, A. Shluger and L. Kantorovich, *J. Phys.: Condens. Matter*, 2010, **22**, 084024.
45 C. Barth and C. R. Henry, *New J. Phys.*, 2009, **11**, 043003.
46 E. Le Moal, M. Müller, O. Bauer and M. Sokolowski, *Phys. Rev. B: Condens. Matter Mater. Phys.*, 2010, **82**, 045301.
47 K. W. Clark, S. Qin, X. Zhang and A.-P. Li, *Nanotechnology*, 2012, **23**, 185306.
48 X. Sun and F. Silly, *Appl. Surf. Sci.*, 2010, **256**, 2228–2231.
49 L. Ch, U. Zerweck, L. M. Eng, S. Gemming, G. Seifert, C. Olbrich, K. Morawetz and M. Schreiber, *Nanotechnology*, 2006, **17**, 1568.
50 S. Silvia and S. Wolf-Dieter, *J. Phys.: Condens. Matter*, 2004, **16**, R49.
51 A. Hauschild, R. Temirov, S. Soubatch, O. Bauer, A. Schöll, B. C. C. Cowie, T. L. Lee, F. S. Tautz and M. Sokolowski, *Phys. Rev. B: Condens. Matter Mater. Phys.*, 2010, **81**, 125432.
52 W. Ji, Z.-Y. Lu and H. Gao, *Phys. Rev. Lett.*, 2006, **97**, 246101.
53 Y. Zou, L. Kilian, A. Schöll, T. Schmidt, R. Fink and E. Umbach, *Surf. Sci.*, 2006, **600**, 1240–1251.
54 W. Ji, Z.-Y. Lu and H.-J. Gao, *Phys. Rev. B: Condens. Matter Mater. Phys.*, 2008, **77**, 113406.
55 I. Hamada and M. Tsukada, *Phys. Rev. B: Condens. Matter Mater. Phys.*, 2011, **83**, 245437.

56 S. Grimme, *J. Comput. Chem.*, 2006, **27**, 1787–1799.
57 S. Grimme, *Wiley Interdiscip. Rev.: Comput. Mol. Sci.*, 2011, **1**, 211–228.
58 P. E. Blöchl, *Phys. Rev. B: Condens. Matter Mater. Phys.*, 1994, **50**, 17953.
59 J. P. Perdew, K. Burke and M. Ernzerhof, *Phys. Rev. Lett.*, 1996, **77**, 3865–3868.
60 B. Hammer, L. B. Hansen and J. K. Nørskov, *Phys. Rev. B: Condens. Matter Mater. Phys.*, 1999, **59**, 7413–7421.
61 G. Kresse and J. Furthmüller, *Comput. Mater. Sci.*, 1996, **6**, 15–50.
62 G. Kresse and D. Joubert, *Phys. Rev. B: Condens. Matter Mater. Phys.*, 1999, **59**, 1758–1775.
63 Z.-X. Hu, H. Lan and W. Ji, *Sci. Rep.*, 2014, **4**, 5036.
64 A. Zangwill, *Physics at Surfaces*, Cambridge University Press, 1988.
65 G. Yu, J. Gao, J. C. Hummelen, F. Wudl and A. J. Heeger, *Science*, 1995, **270**, 1789–1791.
66 R. M. Williams, J. M. Zwier and J. W. Verhoeven, *J. Am. Chem. Soc.*, 1995, **117**, 4093–4099.
67 Y. He, H.-Y. Chen, J. Hou and Y. Li, *J. Am. Chem. Soc.*, 2010, **132**, 1377–1382.
68 N. Martín, L. Sánchez, B. Illescas and I. Pérez, *Chem. Rev.*, 1998, **98**, 2527–2548.
69 E. Sanville, S. D. Kenny, R. Smith and G. Henkelman, *J. Comput. Chem.*, 2007, **28**, 899–908.
70 J. Vogt and H. Weiss, *Surf. Sci.*, 2002, **501**, 203–213.

